

# Metasurface Incorporated Frequency Reconfigurable Planar Antenna for Wireless Applications

Navneet Kaur<sup>1, \*</sup>, Jagtar S. Sivia<sup>2</sup>, and Rajni<sup>3</sup>

**Abstract**—In this paper, the design of a Metasurface incorporated Frequency Reconfigurable Planar Antenna (MS-FRPA) for Wireless Applications is presented. The structure of the projected MS-FRPA consists of a patch with a metasurface placed one above the other with no gap between them. The MS is composed of an array of alternately placed dual split ring resonators arranged periodically in both horizontal and vertical directions. Frequency reconfiguration is achieved by rotating the MS relative to the designed patch antenna. The projected reconfigurable antenna is constructed on Rogers RO4350B material with thickness 1.524 mm. High Frequency Structure Simulator software is employed for analysis of the structure. The results clearly reveal that frequency tuning is achieved in 4.35 to 5.33 GHz with a fractional tuning range of 20.2%. The proposed structure provides appreciable realized gain with stable radiation patterns at all rotation angles. Further, the measured outcomes of the developed prototype show good correlation with the simulated outcomes.

## 1. INTRODUCTION

In the past few decades, a prodigious development has been observed in various systems such as radio-frequency and microwaves due to widespread multi-functionality of wireless communication devices [1–4]. The recent research mainly pays attention towards developing smart systems having potential to perform multiple operations in one device as compared to traditional single operational device [5–7] due to reduction of multipath fading, augmented channel properties, and being resistant to interrupting signals. All these characteristics prompt the development of reconfigurable antennas in present-day wireless communication systems. These antennas have the capacity to reconfigure the important characteristics like frequency, polarization, radiation pattern, and combination of two characteristics or all three [8]. Out of these, frequency reconfigurable antennas are widely preferred as they have the ability to resonate at multiple tuning frequencies [9]. A large number of frequency reconfigurable antennas have been designed and published so far by deploying the electrical methods using positive intrinsic negative (PIN) diodes, varactor diodes, and radiofrequency micromechanical systems (RF-MEMS) & mechanical tuning methods using actuator and large reflector antennas [10, 11]. However, they possess some drawbacks such as requirement of biasing lines and direct current (DC) electrical sources which in turn degrades their performance.

In recent years, to deal with the above discussed hitches, a few accomplishments are made in the exploration of reconfigurability using other means such as metamaterials. Metamaterials are synthetically designed material that displays some notable unnatural electromagnetic (EM) properties which have broadened its importance towards numerous significant applications in science, technology, and medicine. A two-dimensional equivalent of metamaterials is metasurface formed by periodically

---

*Received 27 May 2021, Accepted 4 July 2021, Scheduled 9 July 2021*

\* Corresponding author: Navneet Kaur (navsandhu31696@gmail.com).

<sup>1</sup> Department of Electronics and Communication Engineering, Punjabi University, Patiala, Punjab, India. <sup>2</sup> YCoE, Punjabi University Guru Kashi Campus, Talwandi Sabo, Bathinda, Punjab, India. <sup>3</sup> Shaheed Bhagat Singh State Technical Campus, Ferozepur, Punjab, India.

arranging the array of electrically small scatterers or holes in the form of rings [12]. They occupy less Euclidean space and provide lossless structures in comparison to their 3-D counterparts. Several works have been reported in literature based on this. In [10], the performance of a metasurface based frequency reconfigurable antenna is analyzed by periodically arranging the rectangular loop unit cells atop the patch antenna. A similar idea is demonstrated in [13] to acknowledge a frequency tunable slot antenna with a bidirectional radiation pattern. A meandered unit cell structure based frequency tunable slot antenna is designed in [14]. Though wide tuning range is achieved, there exists a gap between the antenna and MS layer. A frequency reconfigurable antenna is demonstrated in [15] in which elliptical-shaped unit cells are utilized for designing. Frequency and polarization reconfigurability using double layer metasurface is demonstrated in [16]. Li et al. in [17] proposed an equivalent radially homogenous model for a metasurface enabled frequency slot reconfigurable antenna. Wire type unit cells were opted for designing the MS and to estimate the central frequencies with enhanced accuracy, simplicity, and robustness.

Keeping this in view, the aim of this paper is to design a metasurface incorporated frequency reconfigurable planar antenna for wireless applications. The manuscript is presented in five sections. Section 2 illustrates the topology of reconfigurable antenna along with its geometrical details. A metamaterial unit cell is analyzed for EM characteristics in Section 3. The performance results of projected MS-FRPA are elucidated in Section 4. The comparative performance of proposed antenna with other existing antennas is discussed in this section. The work is concluded in Section 5.

## 2. TOPOLOGY OF PROJECTED MS-FRPA

The layout of the projected MS-FRPA is demonstrated in Fig. 1. The structure of the projected MS-FRPA is designed using two substrate layers: one for patch antenna and the other for metasurface. On the top of lower substrate, a rectangle-shaped patch antenna is designed, and on its bottom, a circle-shaped ground plane is implemented using planar technology. The geometrical view of the patch antenna is demonstrated in Fig. 1(a). An array of unit cells of alternately placed dual split ring resonators (DSRRs) joined with thin wire represents the proposed MS. The whole arrangement is designed on the top of the upper substrate as illustrated in Fig. 1(b). In order to achieve frequency reconfigurability of an antenna, MS is rotated across its centre with reference to the designed patch antenna. The rotation angle  $\theta_r$  is evaluated along the  $y$ -axis. The unit cells exhibit similarity in both horizontal and vertical directions. Therefore, it is noticed that  $\theta_r = -\theta_r$ , and its maximum value considered is  $90^\circ$ . During the manufacturing of the antenna structure, the radiating side of the lower substrate and non-radiating side of upper substrate are placed together. Between the two substrates there is no gap present thereby resulting in a compact structure. The side view of the two-layered MS-FRPA structure is shown in Fig. 1(c). For the implementation of designed structure, Rogers RO4350B material with dielectric constant ( $\epsilon_r$ ) of 3.48, loss tangent ( $\tan \delta$ ) of 0.0037, and thickness ( $h$ ) of 1.524 mm is selected for both the substrates. A SubMiniature version A (SMA) connector of  $50 \Omega$  impedance is chosen for proper impedance matching. The photographic view of fabricated prototype of the patch & metasurface and the pictorial view of MS-FRPA is illustrated in Fig. 1(d) and Fig. 1(e), respectively. Table 1 shows the optimized parameters of the projected reconfigurable antenna.

**Table 1.** Parametric description of MS-FRPA (units in mm).

| D  | $L_p$ | $W_p$ | $P_e$ | s   |
|----|-------|-------|-------|-----|
| 39 | 16    | 12    | 2     | 2.4 |

## 3. ANALYSIS OF METAMATERIALISTIC BEHAVIOR

The simulation model of a  $3 \times 3$  DSRR array is placed inside a waveguide medium with boundary conditions and excitations applied along respective faces. The boundary conditions: perfect electric

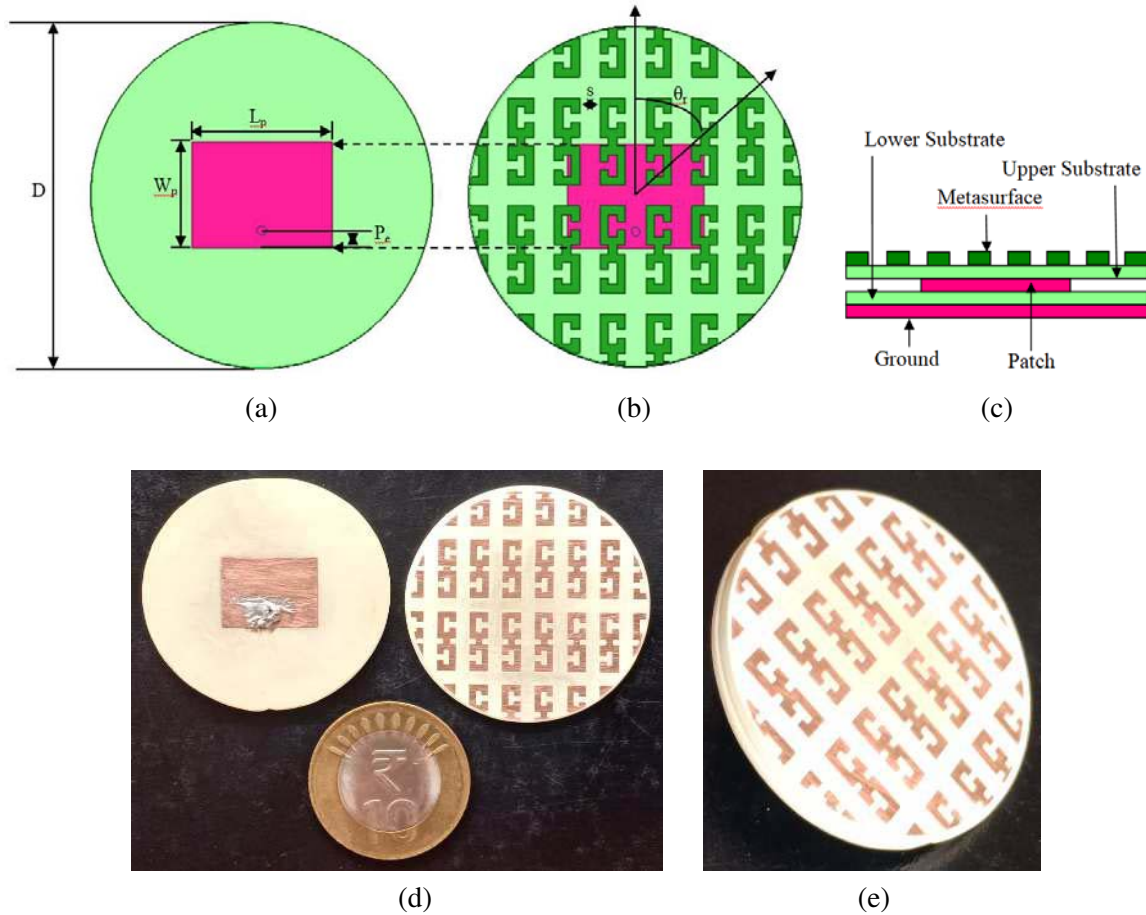


**Figure 1.** Geometrical structure of (a) patch antenna, (b) metasurface, (c) side view, (d) fabricated prototype of patch antenna and metasurface, (e) MS-FRPA.

conductor (PEC) and perfect magnetic conductor (PMC) boundary conditions are applied along the  $z$ - and  $y$ -faces of the unit cell. On the  $x$ -faces from  $-x$  to  $+x$  direction, the two wave ports 1 and 2 are allocated. Thus, a triad of  $E$ - $H$  and  $k$  is created [18–20]. Ansys High Frequency Structure Simulator (HFSS) software is deployed for simulating the structure and to characterize the EM properties of the synthesized material. This behaviour is confirmed by examining the phase reversal characteristics of reflection coefficient ( $S_{11}$ ) and transmission coefficient ( $S_{21}$ ). The enlarged form of unit cell is shown in Fig. 2(a). The structure of SRR generally consists of two metallic rings with a gap in between. Whenever a current moves inside the coil, a magnetic dipole moment is generated. This dipole moment vector is perpendicular to the coil plane. Thus, the coil and capacitor generate an LC circuit with increased dipole moment at the resonance. Thus, the SRR works like an LC circuit with metallic ring and gap representing the inductor (L) and parallel plate capacitor (C), respectively [21, 22]. The LC equivalent circuit of the DSRR is depicted in Fig. 2(b). The geometrical description of DSRR unit cell is tabulated in Table 2.

Figure 3 specifies the transmission and reflection coefficients of the metamaterial structure with

**Table 2.** Parametric description of DSRR (units in mm).

| $U_a$ | $U_b$ | $a$ | $b$ | $c$ | $d$ | $e$ |
|-------|-------|-----|-----|-----|-----|-----|
| 12.4  | 5.4   | 10  | 3   | 4.5 | 1   | 1   |

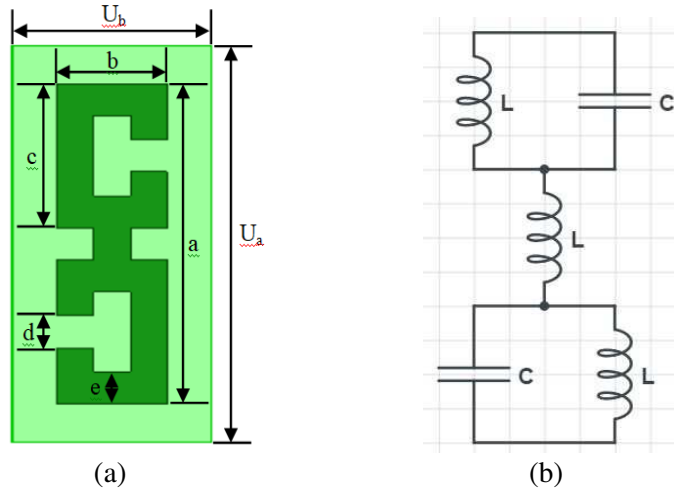


Figure 2. (a) Enlarged unit cell, (b) LC equivalent structure.

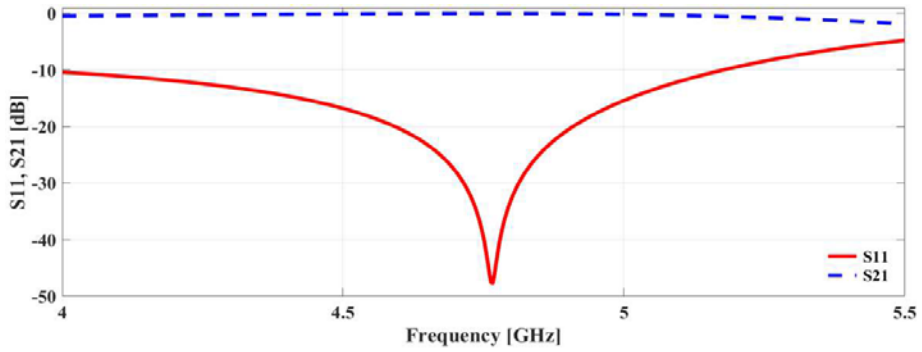


Figure 3. Reflection coefficient ( $S_{11}$ ) and transmission coefficient ( $S_{21}$ ) of the proposed structure.

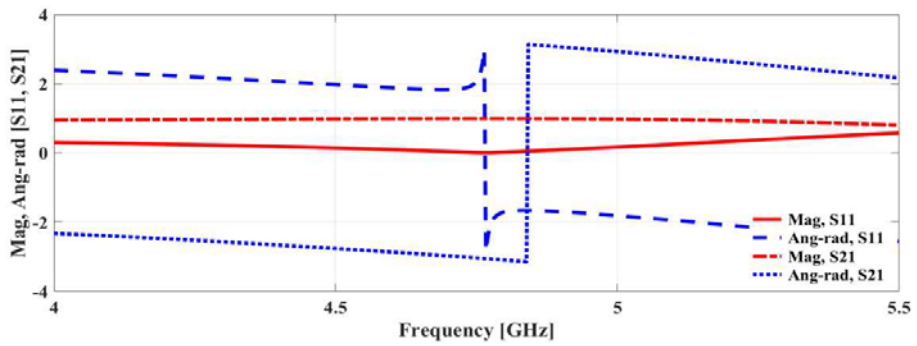


Figure 4. Magnitude and phase response of  $S_{11}$  and  $S_{21}$ .

respect to frequency. The structure reveals the maximum reflection at 47.67 dB below 0 dB. Figure 4 depicts the magnitude and phase angle plots of  $S_{11}$  and  $S_{21}$ . The magnitude curve and phase curve represent the group velocity and phase velocity, respectively. The phase reversal response at particular frequency indicates the metamaterial behaviour of the proposed structure [21]. The negative characteristics of permeability and permittivity are evaluated with the help of real and imaginary parts of  $S_{11}$  and  $S_{21}$ . Nicolson Ross Weir approach is implemented using Matrix Laboratory (MATLAB) for characterizing the values of effective parameters, i.e., permeability and permittivity with  $S_{11}$  and

$S_{21}$  [18]. It is expressed mathematically with the help of following Eqs. (1) to (4)

$$V_1 = S_{21} + S_{11} \tag{1}$$

$$V_2 = S_{21} - S_{11} \tag{2}$$

$$\mu_r = \frac{2}{jk_0d} \frac{1 - V_2}{1 + V_2} \tag{3}$$

$$\epsilon_r = \frac{2}{jk_0d} \frac{1 - V_1}{1 + V_1} \tag{4}$$

where  $V_1$  and  $V_2$  represent the composite terms that express the sum and difference of  $S_{11}$  and  $S_{21}$  of scattering parameters;  $k_0$  specifies the free space wave number;  $d$  denotes the thickness of substrate;  $\mu_r$  and  $\epsilon_r$  signify the effective permeability and permittivity of metamaterial.

The real and imaginary parts of effective parameters are illustrated in Fig. 5. The permeability and permittivity has negative frequency regions from 4.0 to 4.92 GHz and 4.0 to 4.81 GHz as shown in Fig. 5 and Table 3, respectively. The effective parameters are simultaneously negative between 4.0 and 4.81 GHz frequency range. The real value of refractive index is also negative in this frequency range. Thus, the proposed  $3 \times 3$  array of DSRRs behaves as a left-handed medium where the real parts of both permittivity and permeability are negative.

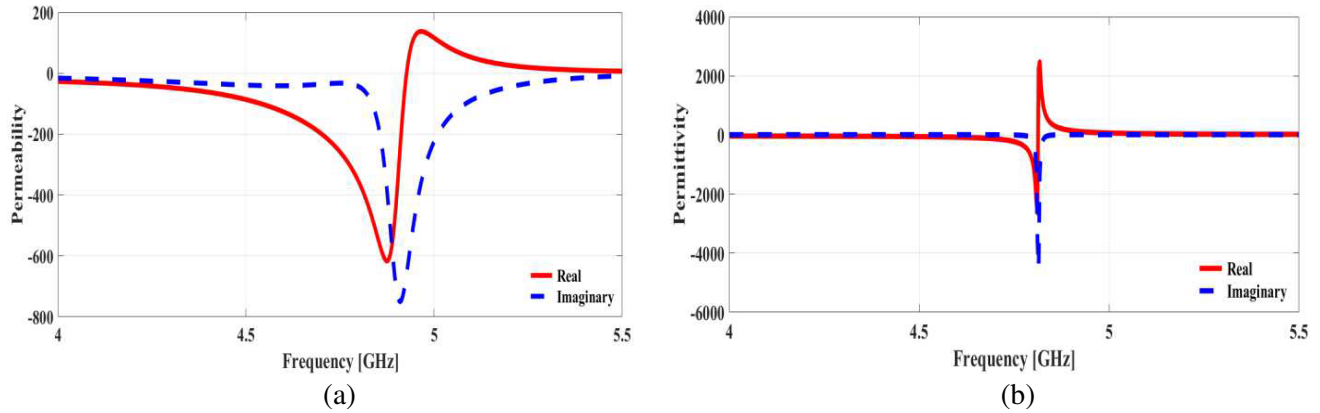


**Figure 5.** Real and imaginary parts of effective parameters (a) permeability, and (b) permittivity.

**Table 3.** Negative index frequency region of effective parameters.

| Parameters                    | Negative index frequency region (in GHz) |
|-------------------------------|--|
| Permeability ( $\mu_r$ )      | 4.0–4.92                                 |
| Permittivity ( $\epsilon_r$ ) | 4.0–4.81                                 |

#### 4. RESULTS AND DISCUSSION

The design and analysis of the projected antenna is done using full wave electromagnetic solver HFSS V15. The structure of fabricated prototype is tested using vector network analyzer (VNA) Anritsu MS46322A.

##### 4.1. Projected DSRR Frequency Reconfiguration

The simulated and measured results of  $S_{11}$  presented in Fig. 6 reveal a noble trend over all frequencies. The resonant frequency increases continuously from 4.35 to 4.72, 5.09, and 5.33 GHz as the rotation

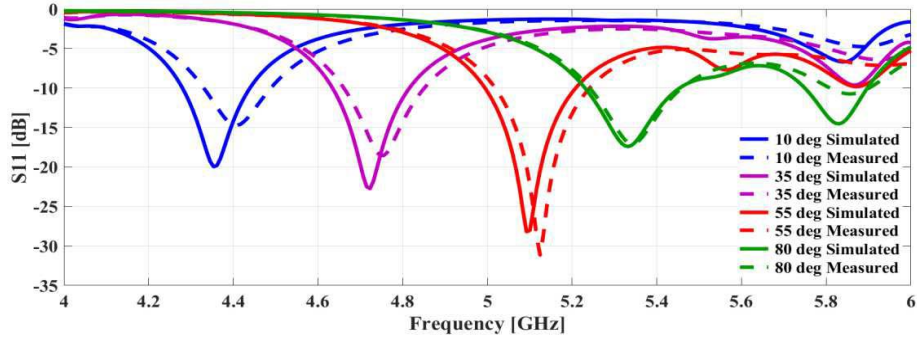


**Figure 6.** Simulated and measured  $S_{11}$  at different rotation angles.

angle changes its value from  $10^\circ$  to  $35^\circ$ ,  $55^\circ$ , and  $80^\circ$ , respectively. The best matching condition occurs at 5.09 GHz that corresponds to  $55^\circ$  rotation angle. The resulting condition degrades as the rotation angle moves away from  $55^\circ$ . The simulated and measured results of reflection coefficient at various rotation angles are shown in Table 4. A reasonable agreement is seen between the simulated and experimentally observed values. Small discrepancies occur among these values and are mainly due to fabrication tolerances, cable effects, environmental conditions, and SMA connector losses.

**Table 4.** Simulated and measured results of reflection coefficient at different rotation angles.

| Rotation angle | Simulated       |                        | Measured        |                        |
|----------------|-----------------|------------------------|-----------------|------------------------|
|                | Frequency (GHz) | Reflection coefficient | Frequency (GHz) | Reflection coefficient |
| $10^\circ$     | 4.35            | -19.9617               | 4.40            | -14.7277               |
| $35^\circ$     | 4.72            | -22.7394               | 4.75            | -18.5627               |
| $55^\circ$     | 5.09            | -28.1995               | 5.12            | -31.1497               |
| $80^\circ$     | 5.33            | -17.4077               | 5.34            | -17.0907               |

The relation between rotation angle and resonant frequency can be analyzed from the graph when  $\theta$  increases from  $10^\circ$  to  $80^\circ$ . The resonant frequency exhibits a linear relationship with the rotation angle. This relation can be approximated using linear regression analysis as shown in Fig. 7. The simulated and measured results display desirable agreements. Thus, as the rotation angle extends from  $10^\circ$  to  $80^\circ$ , the resonant frequency increases consistently from 4.35 to 5.33 GHz resulting in fractional tuning range of 20.2%.

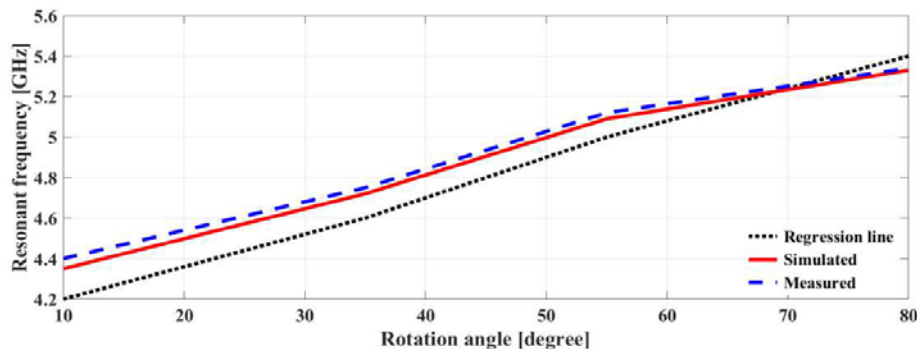


**Figure 7.** Resonant frequency versus rotation angle.

### 4.2. Parametric Analysis

The operational performance of an antenna is examined by varying optimized dimensions of unit cell for carrying out the parametric analysis of the proposed antenna. This study observes four different cases: varying parameters ‘*a*’, ‘*b*’, ‘*c*’, and ‘*s*’ of unit cell. The effect of parameter ‘*a*’ on reflection coefficient is shown in Fig. 8(a). It is visualized from this plot that when the value of parameter ‘*a*’ is increased to 11 mm and 12 mm, the resonant frequency shifts to the higher side. By decreasing the value of parameter ‘*a*’ to 8 mm and 9 mm, the resonant frequency shifts to the lower side. The variation of reflection coefficient with respect to parameter ‘*b*’ is illustrated in Fig. 8(b). From this figure, it is noticed that when the value of parameter ‘*b*’ is increased to 4 mm and 5 mm, the resonant frequency shifts towards lower frequencies, whereas when the value of parameter ‘*b*’ is decreased to 1 mm and 2 mm, the resonant frequency shifts towards the higher frequencies. The variation of parameter ‘*c*’ on reflection coefficient is elucidated in Fig. 8(c). When the value of parameter ‘*c*’ is increased to 5.5 mm and 6.5 mm, the resonant shifts towards the lower level, whereas on decreasing it to 3.5 mm and 2.5 mm, the resonant frequency shifts towards upper levels. The influence of parameter ‘*s*’ on reflection coefficient is elucidated in Fig. 8(d). From this figure, it is analyzed that when the value of ‘*s*’ changes from 2.4 to 3.4 mm and 4.4 mm, the resonant frequency is shifted towards the higher frequencies, whereas when the value changes from 2.4 to 1.4 mm and 0.4 mm, the resonant frequency is shifted towards the lower frequencies.

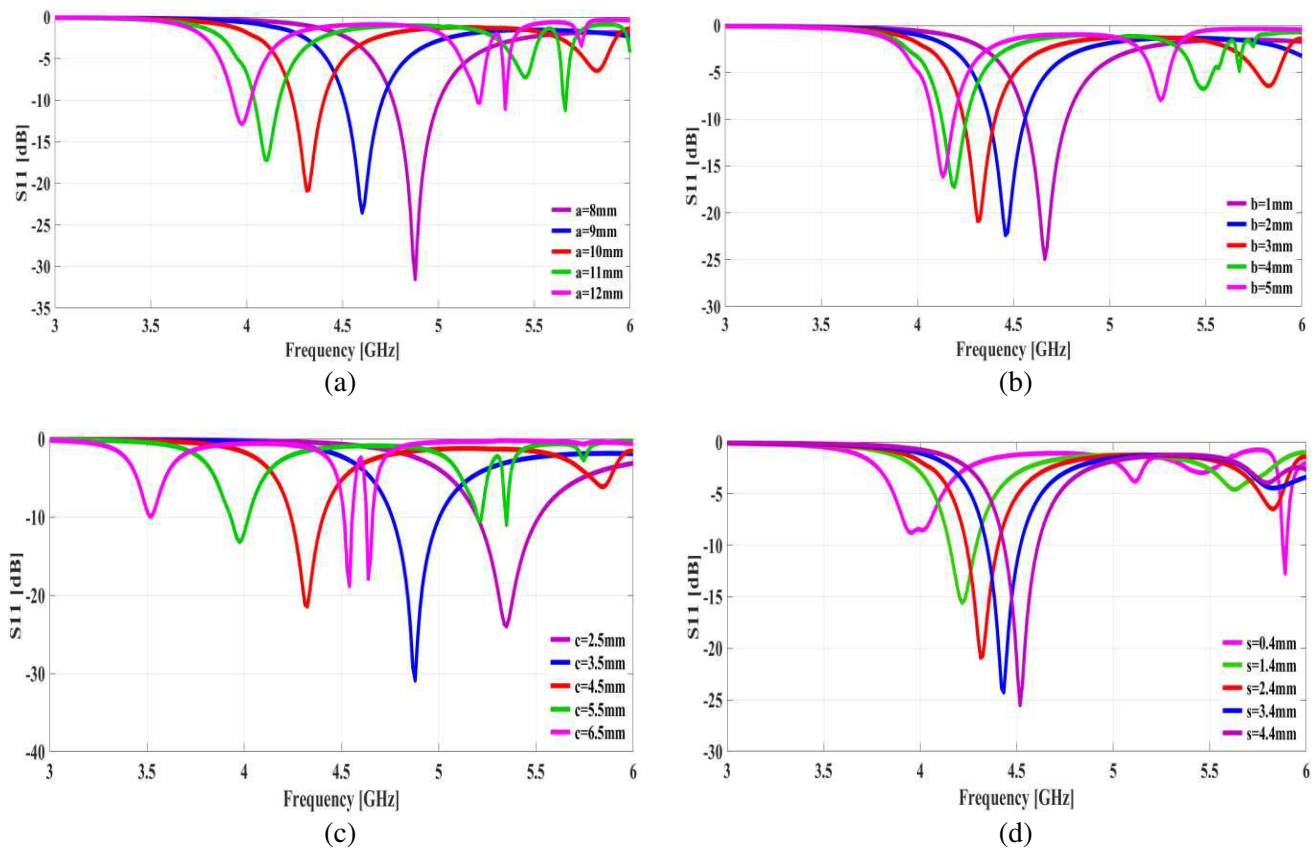


**Figure 8.** (a) Effect of parameter ‘*a*’ on reflection coefficient, (b) effect of parameter ‘*b*’ on reflection coefficient, (c) effect of parameter ‘*c*’ on reflection coefficient, (d) effect of parameter ‘*s*’ on reflection coefficient.

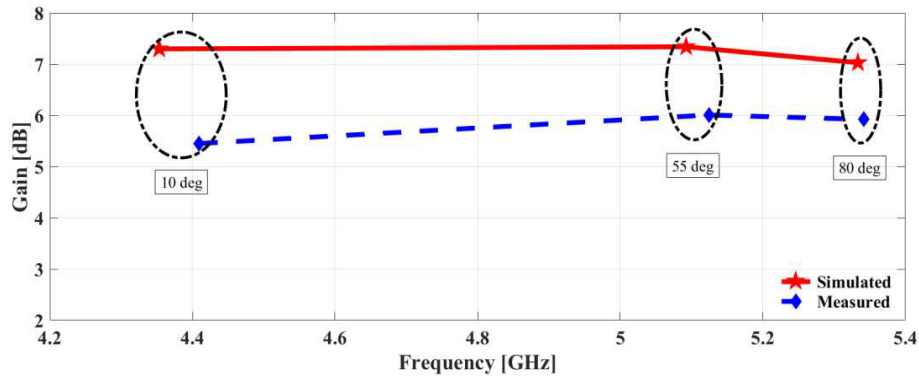


**Figure 9.** Gain versus frequency at different rotation angles.



**Figure 10.** Projected antenna in an anechoic chamber.

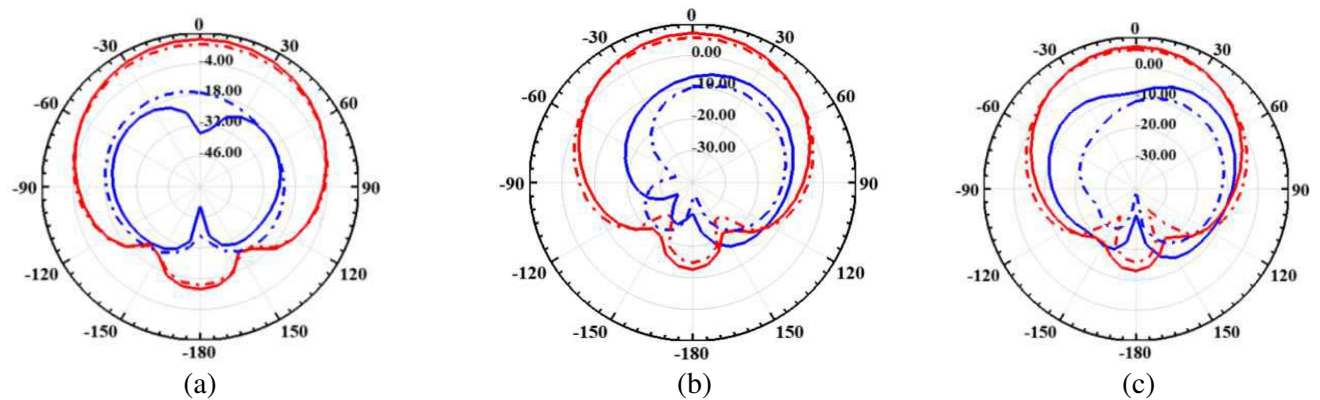


**Figure 11.** Simulated (bold line) and measured (dotdashed line) radiation patterns in  $zx$  plane at rotation angles (a)  $10^\circ$ , (b)  $55^\circ$ , (c)  $80^\circ$  (The red line indicates co-polarization and the blue line signifies cross-polarization).

### 4.3. Gain and Radiation Pattern of Projected MS-FRPA

The important antenna parameters such as gain and radiation pattern are described here at different resonating frequencies in correspondence to rotation angles  $10^\circ$ ,  $55^\circ$ , and  $80^\circ$ . The simulated and measured graphs of gain versus frequency are shown in Fig. 9. From the results, it is observed that gains around 7.29, 7.33, and 7.02 dB have been achieved corresponding to resonant frequencies 4.35 GHz, 5.09 GHz, and 5.33 GHz, respectively. The projected antenna placed in an anechoic chamber is shown

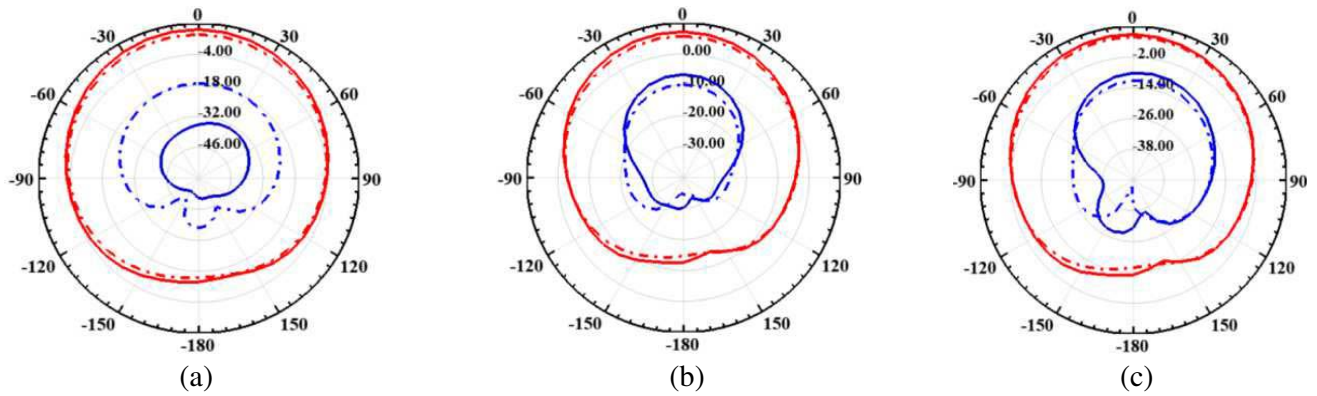


**Figure 12.** Simulated (bold line) and measured (dotdashed line) radiation patterns in  $yz$  plane at rotation angles (a)  $10^\circ$ , (b)  $55^\circ$ , (c)  $80^\circ$  (The red line denotes co-polarization and the blue line specifies cross-polarization).

**Table 5.** Performance comparison of the projected antenna with the other reported reconfigurable antennas.

| Reference No.               | [10]      | [13]      | [14]             | [16]                       | [17]  | Projected antenna |
|-----------------------------|-----------|-----------|------------------|----------------------------|---|-------------------|
| Overall size (mm)           | 40        | 50        | $105 \times 105$ | -                          | 50  | 39                |
| Tuning Range (GHz)          | 4.76–5.51 | 2.78–3.2  | 1.9–2.3          | 4–4.35                     | 3.97–4.74, 3.84–4.55 (ellipse) and 3.82–4.87 (wire) | 4.35–5.33         |
| Bandwidth (MHz)             | 750       | 420       | -                | 350                        | -   | 980               |
| Fractional Tuning Range (%) | 14.6      | 14        | 19               | 8.4                        | 21.1, 18.9 (ellipse) and 24.2 (wire)                | 20.2              |
| Realized Gain               | > 5 dBi   | 4.8 dBi   | 5 dBi            | 5 dBi                      |   | > 7 dB            |
| Reconfigurability type      | Frequency | Frequency | Frequency        | Frequency and polarization | Frequency   | Frequency         |

in Fig. 10. Figs. 11 and 12 show the simulated and measured results of radiation pattern at frequencies 4.35 GHz, 5.09 GHz, and 5.33 GHz in  $zx$  and  $yz$  planes respectively with different rotation angles. The radiation pattern plots indicate that the co-polarization (linear polarization observed along  $y$ -axis) radiates highly as compared to cross-polarization (linear polarization observed along  $x$ -axis). The cross polarization component shows maximum value when the dual split ring resonator gaps are placed orthogonal to each other. Thus, as the rotation angle  $\theta$  varies from  $10^\circ$  towards  $80^\circ$ , gradual increase in cross polarization transmission amplitude is observed [23]. The value of front to back ratio examined is also more than 20 dB at all rotation angles. The simulated radiation efficiencies observed are also greater than 94% at all rotation angles. Thus, metasurface only shifts the frequency of operation without much affecting the shape of radiation pattern and polarization at different rotation angles.

A brief comparison of various performance parameters of projected MS-FRPA with the other reported antennas is shown in Table 5. It is observed that the designed antenna structure exhibits better performance in terms of size, tuning range, gain, and bandwidth.

## 5. CONCLUSION

The design of a metasurface incorporated planar frequency reconfigurable antenna printed on a Rogers RO4350B substrate is presented in this manuscript. Alternately placed dual split ring resonators joined by a thin wire representing the MS are used to reconfigure the frequency. A unit cell structure of DSR is placed inside a waveguide medium to analyze the phase reversal behavior of metamaterial. By rotating the MS relative to the designed patch antenna, it is possible to reconfigure continuously the antenna's operating frequency from 4.35 GHz to 5.33 GHz range resulting in fractional tuning range of 20.2% and bandwidth of 980 MHz without much affecting the shape of the radiation pattern and polarization of the antenna. The proposed structure also provides acceptable gain results.

## ACKNOWLEDGMENT

The authors would like to thank Rogers Corporation for providing support material for fabricating the antenna prototype, National Institute of Technical Teachers Training and Research (NITTTR), Chandigarh and Indian Institute of Technology (IIT), New Delhi for providing the facility to test the fabricated prototype.

## REFERENCES

1. Sabapathy, T., M. F. Bin Jamlos, R. B. Ahmad, M. Jusoh, M. I. Jais, and M. R. Kamarudin, "Electronically reconfigurable beam steering antenna using embedded RF PIN based parasitic arrays (ERPPA)," *Progress In Electromagnetics Research*, Vol. 140, 241–261, 2013.
2. Bhangi, I. K. and J. S. Sivia, "Minkowski and Hilbert curves based hybrid fractal antenna for wireless applications," *International Journal of Electronics and Communications*, Vol. 85, 159–168, Feb. 2018.
3. Sivia, J. S., A. P. S. Pharwaha, and T. S. Kamal, "Analysis and design of circular fractal antenna using artificial neural networks," *Progress In Electromagnetics Research B*, Vol. 56, 251–267, 2013.
4. Singh, J., A. P. Singh, and T. S. Kamal, "Estimation of resonant frequency of a circular microstrip antenna using artificial neural network," *Journal of the Institution of Engineers (India): Series B*, Vol. 93, No. 1, 7–13, Mar.–May 2012.
5. Ge, L. and K. M. Luk, "Frequency-reconfigurable low-profile circular monopolar patch antenna," *IEEE Transactions on Antennas and Propagation*, Vol. 62, No. 7, 3443–3449, Jul. 2014.
6. Kaur, K. and J. S. Sivia, "A compact hybrid multiband antenna for wireless applications," *Wireless Personal Communications*, Vol. 97, No. 4, 5917–5927, Dec. 2017.
7. Bhatia, S. S. and J. S. Sivia, "On the design of fractal antenna array for multiband applications," *Journal of the Institution of Engineers (India): Series B*, Vol. 100, 471–476, May 2019.
8. Anantha, B., L. Meregu, and P. V. D. S. Rao, "A novel single feed frequency and polarization reconfigurable microstrip patch antenna," *International Journal of Electronics and Communications*, Vol. 72, 8–16, Feb. 2017.
9. Li, T., H. Zhai, and C. H. Liang, "Frequency reconfigurable bow-tie antenna array," *Electronics Letters*, Vol. 50, No. 18, 1264–1266, Aug. 2014.
10. Zhu, H. L., X. H. Liu, S. W. Cheung, and T. I. Yuk, "Frequency-reconfigurable antenna using metasurface," *IEEE Transactions on Antennas and Propagation*, Vol. 62, No. 1, 80–85, Jan. 2014.
11. Haupt, R. L. and M. Lanagan, "Reconfigurable antennas," *IEEE Antennas and Propagation Magazine*, Vol. 55, No. 1, 49–61, Feb. 2013.
12. Holloway, C. L., E. F. Kuester, J. A. Gordon, J. O. Hara, J. Booth, and D. R. Smith, "An overview of theory and applications of metasurfaces: The two dimensional equivalents of metamaterials," *IEEE Antennas and Propagation Magazine*, Vol. 54, No. 2, 10–35, Apr. 2012.
13. Zhu, H. L., S. W. Cheung, X. H. Liu, Y. F. Cao, and T. I. Yuk, "Frequency reconfigurable slot antenna using metasurface," *The 8th European Conference on Antennas and Propagation (EuCAP)*, 2575–2577, The Hague, Netherlands, Apr. 2014.

14. Chatterjee, J., A. Mohan, and V. Dixit, "A novel frequency reconfigurable slot antenna using metasurface," *IEEE Indian Conference on Antennas and Propagation (InCAP)*, Hyderabad, India, Dec. 16–19, 2018.
15. Zhu, M. and L. Sun, "Design of frequency reconfigurable antenna based on metasurface," *IEEE 2nd Advanced Information Technology, Electronic, and Automation Control Conference (IAEAC)*, Chongqing, China, Mar. 2017.
16. Chen, X. and Y. Zhao, "Dual-band polarization and frequency reconfigurable antenna using double layer metasurface," *International Journal of Electronics and Communications*, Vol. 95, 82–87, Oct. 2018.
17. Li, H., X. Man, and J. Qi, "Accurate and robust characterization of metasurface-enabled frequency reconfigurable antennas by radially homogeneous model," *IEEE Access*, Vol. 7, 122605–122612, Sept. 2019.
18. Sethi, A. and Rajni, "Determination of electromagnetic parameters of a new metasurface comprising of square loop," *Journal of Engineering Science and Technology*, Vol. 13, No. 1, 48–57, 2018.
19. Rajni, R. and A. Marwaha, "Electrically small microstrip patch antenna loaded with spiral resonator for wireless applications," *Wireless Personal Communications*, Vol. 96, No. 2, 2621–2632, Sept. 2017.
20. Sharma, N. and S. S. Bhatia, "Double split labyrinth resonator-based CPW-fed hybrid fractal antennas for PCS/UMTS/WLAN/Wi-Max applications," *Journal of Electromagnetic Waves and Applications*, Vol. 33, No. 18, 2476–2498, Dec. 2019.
21. Rajni, and A. Marwaha, "Resonance characteristics and effective parameters of new left hand metamaterial," *Telkomnika Indonesian Journal of Electrical Engineering*, Vol. 15, No. 3, 497–503, Sept. 2015.
22. Rajni, R. and A. Marwaha, "An accurate approach of mathematical modeling of SRR and SR for metamaterials," *Journal of Engineering Science and Technology Review*, Vol. 9, No. 6, 82–86, Dec. 2016.
23. Rao, S. J. M., R. Sarkar, G. Kumar, and D. B. Chowdhury, "Gradual cross polarization conversion of transmitted waves in near field coupled planar terahertz metamaterials," *OSA Continuum*, Vol. 2, No. 3, 603–614, Mar. 2019.